Nanoscale

RSC Publishing

PAPER

View Article Online
View Journal | View Issue

Cite this: *Nanoscale*, 2013, **5**, 7505

Reversible switches of DNA nanostructures between "Closed" and "Open" states and their biosensing applications†

Qing-Lin Sheng,[a] Rui-Xiao Liu,[a] Jian-Bin Zheng*[a] and Jun-Jie Zhu[b]

Received 30th March 2013
Accepted 29th May 2013

DOI: 10.1039/c3nr01576a

www.rsc.org/nanoscale

A novel and versatile biosensing platform based on the structural conversion of 3D DNA nanostructures from ET_{DNA} (Equilateral Triangle) to TPF_{DNA} (Triangular Pyramid Frustum) was proposed for the first time. The inputs of aptamers and their relative targets made the DNA structure change from the "Open" to the "Closed" state, leading to the faradaic impedance changes as the output signals. The specific properties of excellent stability and specific rigid structure of 3D DNA nanostructures made the biosensor function as a regenerable, reusable and intelligent platform. The sensor exhibited excellent selectivity for IFN-γ detection with a wide linear range of 1.0×10^{-9} to 2.0×10^{-6} M and a low detection limit of 5.2×10^{-10} M. The distinctive features of DNA nanostructures make them potentially advantageous for a broad range of biosensing, bionanoelectronics, and therapeutic applications.

Introduction

The construction of artificial DNA nanostructures with nearly arbitrary one-, two-, and even three-dimensional (1D, 2D, and 3D) nanostructures has brought us a great revolution in bioelectronics, nanomedicine, molecular computing, nanomachines and biosensors.[1–6] Among the many exciting achievements, molecular circuits based on DNA assembly have the potential to probe systems of biological analytes intelligently and to signal the results of elementary computations on the inputs that they detect autonomously.[7–11]

Despite their often impressive performances, technologies based on DNA assembly on electrode surfaces and their recognition processes suffer from the inherent limitations of stability and irreversibility, which commonly rely on single DNA sequences anchored on electrodes by SH-groups and the recognition relies on DNA hydrolysis,[12–14] or through the use of single-stranded 'toeholds' to initiate strand-displacement reactions.[15–18] To solve these problems, much recent progress has been made in developing 3D DNA architectures.[19,20] Yan and Fan's group have devised a new concept to achieve improved probe–target recognition properties by constructing a "pyramidal" DNA tetrahedra structure-based chip platform. The 3D nanostructured recognition probes anchored on Au surfaces have proven to have mechanical rigidity and structural stability.[21] They also expanded this protocol by adapting a series of DNA structures to DNA tetrahedra and constructed various logic gates, as well as a half-adder operation.[22] The above studies suggest that the protocol for the construction of a versatile biosensing platform based on 3D DNA nanostructures is feasible.

In fact, the integration of reconfigurable DNA nanotechnology into biosensing is a relatively new field that offers great prospects for designing stable, sensitive and selective biosensors. New schemes based on 3D DNA nanostructure-derived bioassays are expected to open new opportunities for DNA nanotechnology, bioelectronics, medical diagnostics and living cell analysis. Herein, we demonstrate the unique reversible conversion of DNA nanostructures between "Closed" and "Open" states and describe their potential in bioanalytical applications.

Experimental

Materials and apparatus

Ethylenediaminetetraacetic acid (EDTA), biotin, bovine serum albumin (BSA), immunoglobulin G (IgG), adenosine 5′-monophosphate (AMP) and dithiothreitol (DTT) were purchased from Sigma-Aldrich (St. Louis, MO). Interferon-γ (IFN-γ), interleukin-6 (IL-6), and tumor necrosis factor-alpha (TNF-α) were obtained from USCNLIFE Company (USA). All other chemicals used in this work were of analytical grade. All oligonucleotides are synthesized by Sangon Biotech. Co., Ltd. (Shanghai, China). Their sequences are listed in Table 1. All oligonucleotides were dissolved with 10.0 mM TE buffer (10.0 mM Tris, 1.0 mM EDTA, pH 7.4) into stock solutions and

[a]*Institute of Analytical Science/Shaanxi Provincial Key Laboratory of Electroanalytical Chemistry, Northwest University, Xi'an, Shaanxi 710069, China. E-mail: zhengjb@nwu.edu.cn; Fax: +86 29 88303448; Tel: +86 29 88373025*

[b]*Key Laboratory of Analytical Chemistry for Life Science of MOE, School of Chemistry and Chemical Engineering, Nanjing University, Nanjing 210093, PR China*

† Electronic supplementary information (ESI) available. See DOI: 10.1039/c3nr01576a

Table 1 Oligonucleotides used in this paper

Group	Name	Sequence
IFN-γ	P1	5′-HS-C6-TATCACCAGGCAGTTGACATTTTTTTTTTTTACACAACAC-3′
	P2	5′-HS-C6-TTCAGACTTAGGAATGTGCTTTTTTTTTTTTCCAACACAA-3′
	P3	5′-HS-C6-TTCCCACGTAGTGTCGTTGTTTTTTTTTTTTCCAACCCCA-3′
	P4	5′-TCAACTGCCTGGTGATATCACGACACTACGTGGGAATGACATTCCTAAGTCTGAA-3′
	P5	5′-TGGGGTTGGTTGTGTTGGGTGTTGTGT-3′
	P3′	5′-HS-C6-TTCCCACGTAGTGTCGTTGTTTTTTTTTTTTCCAACCCCATT-BHQ2-3′
	P5′	5′-Cy3-TTTGGGGTTGGTTGTGTTGGGTGTTGTGT-3′
AMP	Pa1	5′-HS-C6-TATCACCAGGCAGTTGACATTTTTTTTTTTTTGGACCCCC-3′
	Pa2	5′-HS-C6-TTCAGACTTAGGAATGTGCTTTTTTTTTTTTTCATAACGC-3′
	Pa3	5′-HS-C6-TTCCCACGTAGTGTCGTTGTTTTTTTTTTTTCTCCTTCCA-3′
	Pa4	3′-TGGAAGGAGGCGTTATGAGGGGGTCCA-5′
Cocaine	Pc1	5′-HS-C6-TATCACCAGGCAGTTGACATTTTTTTTTTTTTGGGAGACCCACTT-3′
	Pc2	5′-HS-C6-TTCAGACTTAGGAATGTGCTTTTTTTTTTTTCATTGAAGGATTT-3′
	Pc3	5′-HS-C6-TTCCCACGTAGTGTCGTTGTTTTTTTTTTTTATCCTTGTCTCCC-3′
	Pc4	5′-GGGAGACAAGGATAAATCCTTCAATGAAGTGGGTCTCCC-3′

stored at −20 °C. They were diluted with 10.0 mM TE buffer solution to suitable concentrations prior to use. Thiol-modified probes were treated with 0.05 M DTT at room temperature overnight in the dark to reduce the S–S bonds prior to use. The buffer for ET_{DNA} and TPF_{DNA} assembly was 20.0 mM TE (pH 8.0), 50.0 mM $MgCl_2$ and 0.5 M NaCl. The DNA immobilization buffer was 10.0 mM TE (pH 7.4) containing 0.5 M NaCl. The washing buffer was 10.0 mM PB buffer containing 0.1 M NaCl (pH 7.4). The diluent was 0.1 M PBS (pH 7.2). All solutions were prepared with ultrapure water (>18 MΩ cm) obtained from a Millipore Milli-Q water purification system.

Electrochemical experiments were performed with a CHI 660D Electrochemical Workstation (Shanghai Chenhua Instruments Corporation, China). A three-electrode electrochemical cell was used. An Au electrode ($Ø = 2.0$ mm, Shanghai Chenhua Instruments Corporation, China) was used as the working electrode. Platinum wire and a saturated calomel electrode (SCE) were used as counter and reference electrodes, respectively. The atomic force microscope (AFM) was a Digital Instruments Multimode SPM-9500J3 (Shimadzu Corporation, Japan), operating in *ex situ* Tapping Mode. Transmission electron microscopy (TEM) images were acquired with a JEOL JEM-3010 high-resolution transmission electron microscope using an accelerating voltage of 150 kV. The fluorescence measurements were performed on a Hitachi F-4500 fluorescence spectrophotometer.

Formation of ET_{DNA} and TPF_{DNA}

For ET_{DNA} formation: Four oligonucleotides (P1, P2, P3 and P4) in equimolar quantities were mixed in TM buffer (20.0 mM TE, 50 mM $MgCl_2$ and 0.5 M NaCl, pH 8.0); the mixture was heated to 95 °C for 2 min and then cooled to 4 °C in 30 s. For TPF_{DNA} formation: Five oligonucleotides (P1, P2, P3, P4 and P5) in equimolar quantities were mixed in TM buffer (20.0 mM TE, 50 mM $MgCl_2$ and 0.5 M NaCl, pH 8.0); the mixture was heated to 95 °C for 2 min and then cooled to 4 °C in 30 s.

Assembling of ET_{DNA} and TPF_{DNA} on Au electrodes and biosensing applications

The Au electrodes were first polished with aqueous slurries of 0.3 μm and 0.05 μm α-Al_2O_3 powders on a polishing microcloth. Then, the Au electrodes were cleaned in "piranha" solution consisting of a 3 : 1 ratio of H_2SO_4 and H_2O_2 (caution: this mixture reacts violently with organic materials and must be handled with extreme care), then thoroughly washed with ethanol and ultrapure H_2O, and dried under nitrogen. The obtained clean Au electrodes were then immersed in different ET_{DNA} and TPF_{DNA} solutions and incubated for different times (from 0.5 to 10 h) in the dark at 4 °C. Following incubation, the electrodes were rinsed with washing buffer. Thus, the capture ET_{DNA} and TPF_{DNA} modified Au electrodes were used for the following experiments.

The obtained ET_{DNA} modified Au electrode was first incubated in a solution containing 1.0 nM P5 aptamer solution in the immobilization buffer for 3 h at room temperature. Then, the electrode was transferred to the 2.0 nM IFN-γ solution and incubated for 30 min. During each step, the electrode was extensively rinsed and subjected to electrochemical measurements. For biosensing of IFN-γ, the ET_{DNA} modified Au electrode was first incubated in a solution containing 2.0 μM P5 aptamer solution in the immobilization buffer for 3 h at room temperature to ensure all the ET_{DNA} nanostructures changed to TPF_{DNA}. Then the electrode was transferred into different concentrations of IFN-γ solution, after incubation for 30 min, the electrode was extensively rinsed and subjected to electrochemical measurements.

Results and discussion

Feasibility study

To demonstrate the general design of the 3D DNA nanostructure based biosensing platform, we first use IFN-γ and its aptamer as the pair of target–aptamer for a proof of concept. IFN-γ is a cytokine released by the human immune system, and abnormal levels of IFN-γ are related to many infectious disease

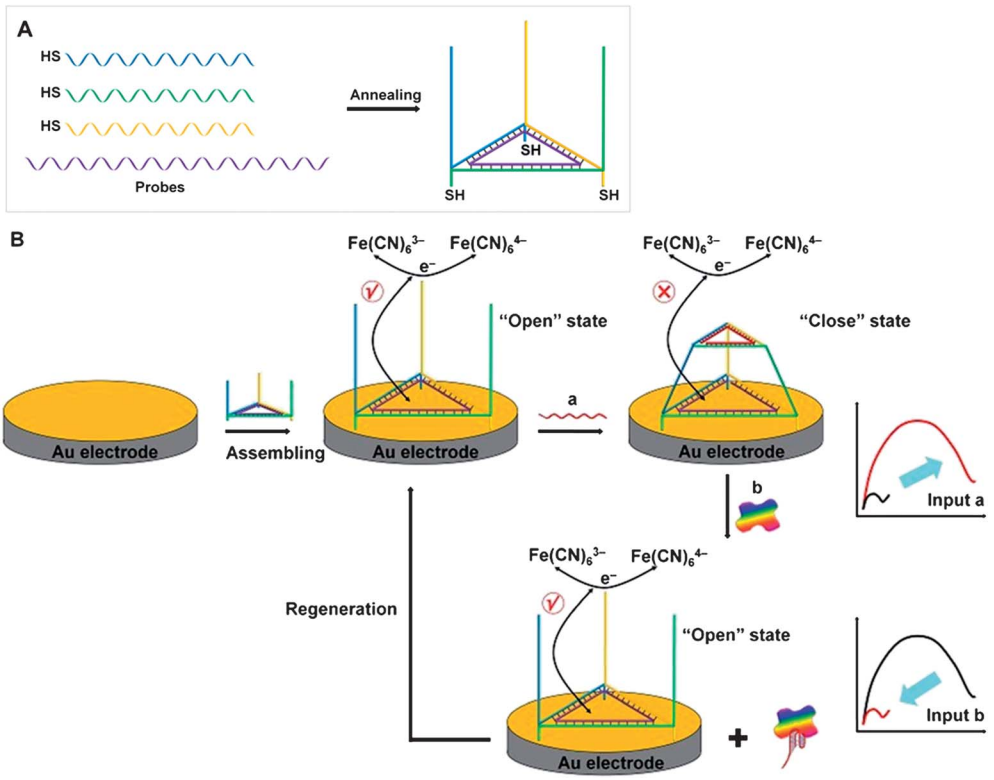

Fig. 1 (A) Schematic illustration of the ET_{DNA} (Equilateral Triangle DNA) nanostructure. The ET_{DNA} was self-assembled in equal stoichiometric amounts of three thiolated 36-nt DNA fragments and one 55-nt DNA fragment. (B) Schematic representation of the biosensing process based on the "Closed" and "Open" states during the conversion between the ET_{DNA} and TPF_{DNA} nanostructures assembled on an Au electrode (a: aptamer, b: target).

and pathogen-directed responses of the human body.[23] Fig. 1 outlines the principle for the construction of 3D DNA nanostructures. 1.0 mM $Fe(CN)_6^{3-/4-}$ was employed as the electron indicator to monitor the "Open" and "Closed" states. The initial Equilateral Triangle DNA nanostructure, defined as ET_{DNA}, is first hierarchically assembled from four stoichiometric equivalents of DNA probes, three thiolated DNA probes (P1, P2, and P3) of 36 nucleotides (40-nt) and one 55-nt DNA probe (P4). Here, the P4 sequence composed of three equal parts of 17-base fragments can specifically bind to the relative 5′-end of the three thiolated probes (all oligonucleotides used in this paper are listed in Table 1). After incubation of an Au electrode in ETDNA solution, the ET_{DNA} film assembled from the three thiol groups on Au electrode surfaces is formed. In this state, the electron transfer of $Fe(CN)_6^{3-/4-}$ is not inhibited and a large current response of $Fe(CN)_6^{3-/4-}$ is obtained. Thus, the ET_{DNA} can represent an "Open" state of the DNA nanostructure. When the ET_{DNA} modified electrode is subsequently incubated in a 27-base IFN-γ aptamer probe (P5) solution, a Triangular Pyramid Frustum nanostructure (defined as TPF_{DNA}) is constructed. Here, the P5 is fully complementary to the 3′-end of the 9-base fragments of thiolated P1, P2, and P3 which allows the formation of a short 9-base DNA duplex at the distal end of the probes. At this stage, the electron transfer of $Fe(CN)_6^{3-/4-}$ is greatly inhibited, due to the formation of the 3D TPF_{DNA} that prevents $Fe(CN)_6^{3-/4-}$ from accessing the electrode surface for efficient electron transfer and a small current response of $Fe(CN)_6^{3-/4-}$ is obtained. Thus, the TPF_{DNA} can represent a "Closed" state of the DNA nanostructure. When the TPF_{DNA} modified electrode is further incubated in a solution containing IFN-γ, the IFN-γ aptamer P5 will be released from the TPF_{DNA} nanostructure and allosteric changes occur to bind IFN-γ, resulting in the "Opening" of the DNA nanostructure. As a result, the TPF_{DNA} nanostructure returns back to the initial ET_{DNA} nanostructure, resulting in an efficient electron transfer and a large current response of $Fe(CN)_6^{3-/4-}$.

Characterization of DNA nanostructures

TEM was first used to characterize the obtained ET_{DNA} and TPF_{DNA} nanostructures, and the results are given in the ESI of Fig. S-1.† Studies show that an edge length of ~6.0 nm of ET_{DNA} with equilateral triangle shapes is observed. For TPF_{DNA}, the edge length and height of ~6.0 nm were also observed. The length and size values of the DNA nanostructures almost coincide with the expected length of DNA in Fig. 1, assuming 0.34 nm per base pair.[24,25] It is necessary to mention here, clear images of the inner structures of the DNA nanostructures are difficult to obtain with high-resolution by current microscopies, due to the small size of the DNA nanostructures used in this study. Analyzing the random selection of the assembled molecules on the Au electrode in the AFM image shows a height of ~6 nm, suggesting the TPF_{DNA} nanostructures have been successfully formed on Au electrode surfaces. The large

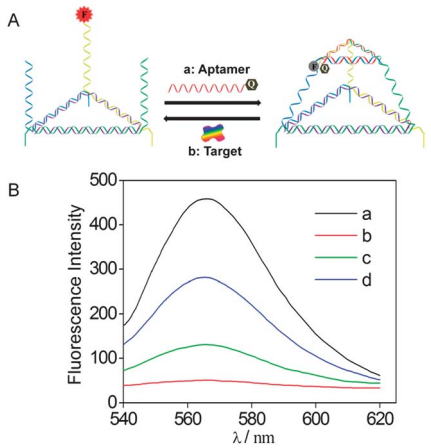

Fig. 2 (A) Scheme of the fluorophore–quencher-based nanostructure conversion reconfigured by the presence of aptamer and target. (B) Fluorescence spectra corresponding to the (a) ET_{DNA} and (b) TPF_{DNA} nanostructures. Curves (c) and (d) show the fluorescence spectra of TPF_{DNA} nanostructures after addition of 2.0×10^{-10} and 2.0×10^{-9} M IFN-γ, respectively.

background of the AFM image is ascribed to the relatively rough substrate of the Au electrode. Besides, when conducting the TEM observation with a high accelerating voltage over 200 kV, the DNA nanostructures would disappear immediately. The disappeared DNA nanostructures of the TEM images can be found in the ESI of Fig. S-2.† Native polyacrylamide gel electrophoresis (PAGE) analysis also further confirmed the assembly of these ET_{DNA} and TPF_{DNA} nanostructures (Fig. S-3†). To test the feasibility of our strategy, fluorescence measurements during the DNA nanostructure conversions were also designed (Fig. 2A). The DNA probe P3′ instead of P3 and IFN-γ aptamer subunits P5′ are used, for which the 3′-ends of P3′ and 5′-ends of P5′ are modified with the BHQ2 quencher and Cy3 fluorophore, respectively. In the absence of P5′, the fluorescence of the ET_{DNA} nanostructure is "On". In the presence of P5′, Cy3 is quenched by BHQ2 due to the formation of the TPF_{DNA} nanostructure and the fluorescence is turned "Off". When IFN-γ is added to the above system, the TPF_{DNA} nanostructure returns back to the initial ET_{DNA} nanostructure, resulting in the generation of fluorescence again (Fig. 2B). The fluorescence changes upon analyzing different concentrations of IFN-γ provide the possibility for quantitative measurement of the target concentration.

Optimization

In order to obtain good assay results, some factors are investigated in detail. It has been proven that the conformational effects are sensitively dependent on the surface densities of the assembled sensing units. The surface density of TPF_{DNA} on the Au electrode is a crucial parameter contributing to signal gain, which can be controlled by varying the probe concentration during the sensor fabrication process. To optimize the signal gain, the performance of the sensors fabricated with different concentrations of TPF_{DNA} (0.1–5.0 μM) was studied under the same concentration of 100 nM target IFN-γ. The change of ΔR_{et} ($\Delta R_{et} = R^0_{et} - R_{et}$) was used to characterize the change of the electrode surface. It was clearly observed that the ΔR_{et} increased with the increase of surface density when the concentration of TPF_{DNA} was 1.0 μM. The surface density of the TPF_{DNA} surface is calculated to be 3.5×10^{12} probe per cm^2. Hence, 1.0 μM TPF_{DNA} is chosen as the optimal concentration for the following experiment. Next, the assembling time of TPF_{DNA} on the Au electrode surface and incubation time of TPF_{DNA} with IFN-γ were checked. It was found that the ΔR_{et} signals increased rapidly for assembling and incubation, and then became saturated at 30 min and 20 min. Thus, 30 min assembling time and 20 min incubation time were used in the standard procedures. For the assembling of ET_{DNA} on the Au electrode surface, factors that influence the conformational effects were also investigated. Results show that a concentration of 1.0 μM ET_{DNA}, an assembling time of 30 min and an incubation time of 20 min are the optimal conditions. The surface density of the ET_{DNA} surface is also calculated to be 3.3×10^{12} probe per cm^2.

Electrochemical investigation

Fig. 3 shows the cyclic voltammograms (CVs) and faradaic impedance spectra (FIS) of the modified electrode during the "Open" and "Closed" states. For comparison, CVs and FIS of bare Au electrode were also presented. For bare Au electrode, a pair of well-defined and revisable redox peaks with the reduction and oxidation peak potentials at 0.144 V and 0.215 V (*vs.* SCE) is observed (Fig. 3A, curve a). For the ET_{DNA} modified electrode, the redox peaks become a little irreversible with the reduction and oxidation peak potentials at 0.101 V and 0.248 V (*vs.* SCE), accompanied by the decrease of peak currents (Fig. 3A, curve b). After the formation of TPF_{DNA} on the Au electrode surface, the redox peaks become absolutely irreversible with the reduction and oxidation peak potentials at −0.109 V and 0.418 V (*vs.* SCE), accompanied by the obvious decrease of peak currents (Fig. 3A, curve c). When the TPF_{DNA} modified electrode is further incubated in IFN-γ solution, the redox peaks of the TPF_{DNA} modified electrode switch to almost the same state of ET_{DNA} modified electrode (Fig. 3A, curve d). During this process, the interfacial electron resistance (R_{et}) signal values for both the "Open" and "Closed" states are rather consistent even after five interrogations, suggesting that the

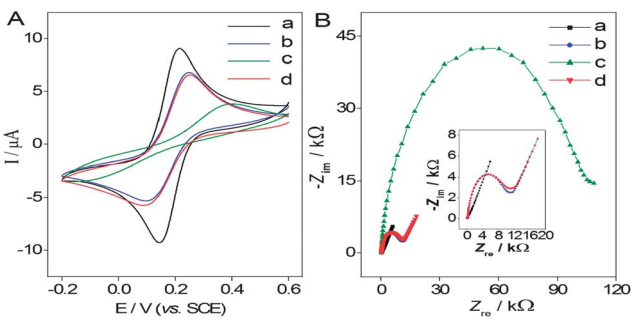

Fig. 3 CVs (A) and FIS (B) of the (a) bare and (b–d) DNA nanostructure modified electrodes in a 1.0 mM $Fe(CN)_6^{3-/4-}$ (containing 0.1 M NaCl) solution. (b) The initial "Open" state of ET_{DNA}, (c) the middle "Closed" state of TPF_{DNA}, and (d) the reset to the "Open" state of ET_{DNA}. Scan rate: 50 mV s^{-1}. Applied potential: +0.179 V (*vs.* SCE). Frequency range: 10 mHz to 10 kHz. Amplitude: 5 mV.

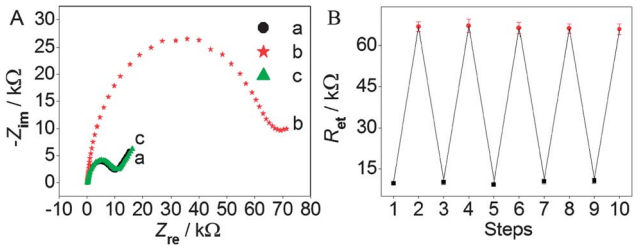

Fig. 4 (A) FIS curves of the reversible changes of the electron-transfer resistance upon "Open"/"Closed" functions. (a) The initial "Open" state of ET_{DNA}, (b) the middle "Closed" state of TPF_{DNA}, and (c) the reset to the "Open" state of ET_{DNA}. The experiment was performed upon application of the biasing potential of +0.179 V (*vs.* SCE). (B) Reversible changes of the R_{et} values upon "Open"/"Closed" functions.

assembled DNA nanostructure owns excellent stability. The electron transfer rate constants (k_s) of $Fe(CN)_6^{3-/4-}$ at the bare Au, ET_{DNA} and TPF_{DNA} modified Au electrodes are 9.391 ± 0.126, 0.551 ± 0.048 and 0.0078 ± 0.0006 s^{-1}, respectively, based on the Laviron theory.[26] This reveals that the k_s values for the ET_{DNA} and TPF_{DNA} modified Au electrodes are approximately 17 and 1200 times lower than that obtained at the bare Au electrode. Thus, FIS may be used as an effective method for probing the features of interfacial electron-transfer resistance during the "Open" and "Closed" process. Fig. 3B shows the FIS of the bare Au (curve a), ET_{DNA} (curve b), and TPF_{DNA} modified Au electrodes before (curve c) and after treatment of the electrodes with IFN-γ (curve d). As can be seen, the addition of P5 probe and IFN-γ made the R_{et} increase and decrease dramatically, which is consistent with the CV results. Thus, the addition of both substrates, aptamer P5 and IFN-γ, results in the activation of both the DNA nanostructure "Open" and "Closed" states and generates the R_{et} corresponding to the status of the DNA nanostructure. Unlike those previous strategies for signal "On/Off" and revisable sensing, the proposed 3D DNA nanostructure system is stable enough to operate for several cycles without significant decay (Fig. 4).

FIS investigation for IFN-γ biosensing

As shown in Fig. 3, if the assembled ET_{DNA} nanostructures on Au electrode surfaces are all switched to TPF_{DNA} *via* the base-pairing interaction among the IFN-γ aptamer and P1, P2, and P3 fragments, the addition of IFN-γ will lead to the release of the IFN-γ aptamer from the electrode surface and a decreased R_{et} value in FIS will be observed. Fig. 5A shows the CVs of the TPF_{DNA} modified Au electrodes in a 1.0 mM $Fe(CN)_6^{3-/4-}$ (containing 0.1 M NaCl) solution corresponding to different concentrations of IFN-γ. It can be seen that with the increase of IFN-γ added in the solution, the oxidation peak potential is negatively shifted and the reduction peak potential is positively shifted, and the peak current increases gradually. Under the optimum conditions, the relationship between the R_{et} value and the concentrations of target IFN-γ was studied (Fig. 5B). $\Delta R/R_{et}^0$ ($(R_{et}^0 - R_{et})/R_{et}^0$) is used for evaluating the concentrations of target IFN-γ. As shown in Fig. 5C, there is a linear relationship between $\Delta R/R_{et}^0$ and the function of the logarithm of the

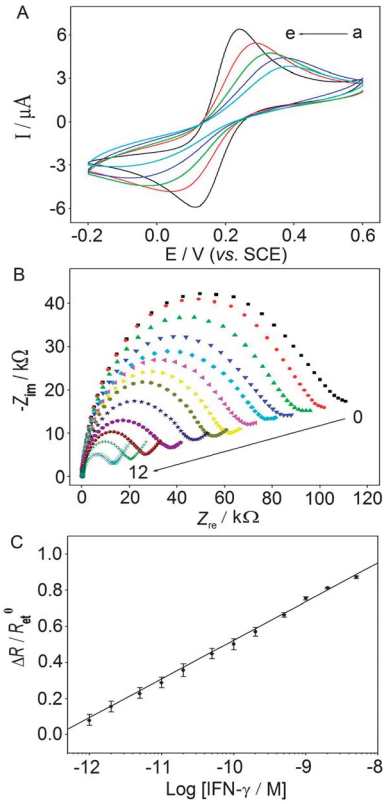

Fig. 5 (A) CVs of the "Closed" state of TPF_{DNA} modified Au electrodes in a 1.0 mM $Fe(CN)_6^{3-/4-}$ (containing 0.1 M NaCl) solution corresponding to (a) 0, (b) 5.0×10^{-12}, (c) 5.0×10^{-11}, (d) 5.0×10^{-10}, and 5.0×10^{-9} M IFN-γ. (B) FIS curves of the TPF_{DNA} modified Au electrodes in a 1.0 mM $Fe(CN)_6^{3-/4-}$ (containing 0.1 M NaCl) solution corresponding to different concentrations of IFN-γ (from 0 to 12: 1.0×10^{-12}, 2.0×10^{-12}, 5.0×10^{-12}, 1.0×10^{-11}, 2.0×10^{-11}, 5.0×10^{-11}, 1.0×10^{-10}, 2.0×10^{-10}, 5.0×10^{-10}, 1.0×10^{-9}, 2.0×10^{-9}, and 5.0×10^{-9} M). (C) The corresponding calibration plot of $\Delta R/R_{et}^0$ *vs.* IFN-γ concentrations.

concentration of IFN-γ over a wide concentration range from 1.0×10^{-12} to 5.0×10^{-9} M ($r = 0.9978$). The detection limit is estimated to be 5.2×10^{-13} M with 3σ (where σ is the relative standard deviation of 6 parallel measurements of the blank solution). This value is lower than some IFN-γ sensors based on fluorescence,[27] surface plasmon resonance[28] and electrochemical detection.[29,30] The sensitivity for IFN-γ detection was

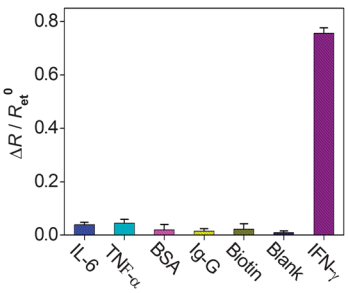

Fig. 6 Specificity of the biosensor for IFN-γ detection over the same concentration of 1.0 nM IL-6, TNF-α, BSA, IgG, and biotin. The error bars represent the standard deviations of triplicate measurements.

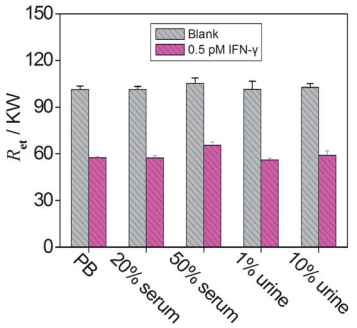

Fig. 7 R_{et} values of the biosensor in blank or 5.0×10^{-10} M IFN-γ within PB, 20% serum, 50% serum, 1% urine and 10% urine samples.

17.4 kΩ/log([IFN-γ]/(10^{-9} M)), which was 9-fold or 17-fold enhancement over other impedimetric biosensors based on RNA or DNA aptamers,[31] indicating the high sensitivity of our proposed sensing system. Furthermore, IL-6, TNF-α, BSA, IgG and biotin showed hardly any change of R_{et} (Fig. 6), indicating that the sensing platform has excellent selectivity and might be a promising tool for IFN-γ assays in real samples.

The sensor was used to detect IFN-γ in 20% and 50% human serum (Fig. 7) diluted with buffer in comparison with those in blank buffer. Studies show that the R_{et} signal decreased of 56.7 and 56.3%, respectively, when 5.0×10^{-10} M IFN-γ were added to 20% and 50% human serum. Moreover, the detection limits were closed to those obtained in blank buffer, suggesting that the other components of the serum did not interfere significantly with sensor performance. Analysis of IFN-γ in 1% and 10% human urine samples was also conducted. As shown in Fig. 7, the R_{et} signals decrease of 55.2% and 58.1%, respectively. Thus, the successful detection of IFN-γ in serum and urine as demonstrated here may be straightforward when testing for IFN-γ clinically.

Exploration investigation of the DNA nanostructure conversion

To demonstrate the generality of the design, adenosine, cocaine and their relative aptamers were also selected for biosensing applications. Similar to the IFN-γ aptamer sensor described above, the adenosine and cocaine aptamers were used as the linker to convert the assembled ET_{DNA} nanostructure to the TPF_{DNA} nanostructure, realizing the "Open" and "Closed" functions. Interestingly, we found that the FIS responses of the assembled TPF_{DNA} on Au electrode for the adenosine aptamer were almost the same as that for the IFN-γ aptamer, under the same conditions. However, the FIS responses for cocaine aptamer-based TPF_{DNA} were smaller than that for the IFN-γ aptamer. We assume the reason for the changes may be ascribed to the length of the IFN-γ aptamer being equal to the adenosine aptamer (27-nt), thus the inhibition of electron transfer between $Fe(CN)_6^{3-/4-}$ and the electrode is similar. While the length of the cocaine aptamer (39-nt) is larger than the IFN-γ aptamer, the top of the formed TPF_{DNA} nanostructure is more "open", and the electron transfer between $Fe(CN)_6^{3-/4-}$ and the electrode becomes easier (Fig. S-8 and Table S-1†).

Conclusion

In summary, a novel biosensing platform based on the "Open" and "Closed" states of 3D DNA nanostructures is presented. The conversion of the DNA nanostructures between ET_{DNA} and TPF_{DNA} is capable of reversible motion in response to an external chemical stimulus. Due to the excellent stability and specific rigid structure of 3D DNA nanostructures, regenerable and reusable functions are realized. Additionally, the significant changes of R_{et} during the "Open" and "Closed" states of DNA nanostructures when aptamers and their relative targets bind to or release from the electrode surface used here can potentially be adapted to the design of sensitive electrochemical or optical biosensors. It can be anticipated that other bioelements with higher affinities to targets, such as RNA or peptides, can also be applied to this strategy, which undoubtedly holds great promise in biosensing, bionanoelectronics, and diagnosis of virus.

Acknowledgements

The authors acknowledge the NSFC (no. 21105080 and 21275116), the SRFDP of China (no. 20126101120023), the Natural Science Foundation of Shaanxi Province of China (no. 2012JQ2010 and 2012JM2013), the Scientific Research Foundation of Shaanxi Provincial Key Laboratory (no. 11JS080 and 12JS087) and the Foundation of Shaanxi Province Educational Committee of China (no. 12JK0576) for financial support.

References

1 C. X. Lin, S. Rinker, X. Wang, Y. Liu, N. C. Seeman and H. Yan, *Proc. Natl. Acad. Sci. U. S. A.*, 2008, **105**, 17626.
2 D. Kang, A. Vallée-Bélisle, A. Porchetta, K. W. Plaxco and F. Ricci, *Angew. Chem., Int. Ed.*, 2012, **51**, 6717.
3 A. Vallée-Bélisle, A. J. Bonham, N. O. Reich, F. Ricci and K. W. Plaxco, *J. Am. Chem. Soc.*, 2011, **133**, 13836.
4 S. Surana, J. M. Bhat, S. P. Koushika and Y. Krishnan, *Nat. Commun.*, 2011, **2**, 340.
5 Z. G. Wang, J. Elbaz and I. Willner, *Nano Lett.*, 2011, **11**, 304.
6 G. Pelossof, R. Tel-Vered, S. Shimron and I. Willner, *Chem. Sci.*, 2013, **4**, 1137.
7 A. J. Genot, J. Bath and A. J. Turberfield, *J. Am. Chem. Soc.*, 2011, **133**, 20080.
8 T. Carell, *Nature*, 2011, **469**, 45.
9 A. Prokup, J. Hemphill and A. Deiters, *J. Am. Chem. Soc.*, 2012, **134**, 3810.
10 M. Zhou, Y. Du, C. G. Chen, B. L. Li, D. Wen, S. J. Dong and E. K. Wang, *J. Am. Chem. Soc.*, 2010, **132**, 2172.
11 M. Zhou, F. Kuralay, J. R. Windmiller and J. Wang, *Chem. Commun.*, 2012, **48**, 3815.
12 T. Ran, S. Kaplan and E. Shapiro, *Nat. Nanotechnol.*, 2009, **4**, 642.

13 C. Carrasquilla, P. S. Lau, Y. F. Li and J. D. Brennan, *J. Am. Chem. Soc.*, 2012, **134**, 10998.
14 F. A. Wang, J. Elbaz, R. Orbach, N. Magen and I. Willner, *J. Am. Chem. Soc.*, 2011, **133**, 17149.
15 L. L. Qian and E. Winfree, *Science*, 2011, **332**, 1196.
16 W. W. Yang and R. Y. Lai, *Chem. Commun.*, 2012, **48**, 8703.
17 S. Shin, B. Y. Won, C. Jung, S. C. Shin, D. Y. Cho, S. S. Lee and H. G. Park, *Chem. Commun.*, 2011, **47**, 6611.
18 D. Soloveichik, G. Seelig and E. Winfree, *Proc. Natl. Acad. Sci. U. S. A.*, 2010, **107**, 5393.
19 S. M. Douglas, H. Dietz, T. Liedl, B. Hogberg, F. Graf and W. M. Shih, *Nature*, 2009, **459**, 414.
20 Z. Li, B. Wei, J. Nangreave, C. X. Lin, Y. Liu, Y. L. Mi and H. Yan, *J. Am. Chem. Soc.*, 2009, **131**, 13093.
21 H. Pei, L. Liang, G. B. Yao, J. Li, Q. Huang and C. H. Fan, *Angew. Chem., Int. Ed.*, 2012, **124**, 91548.
22 H. Pei, N. Lu, Y. L. Wen, S. P. Song, Y. Liu, H. Yan and C. H. Fan, *Adv. Mater.*, 2010, **22**, 4754.
23 H. Pei, L. Liang, G. B. Yang, J. Li, Q. Huang and C. H. Fan, *Angew. Chem., Int. Ed.*, 2012, **51**, 9020.
24 Z. Y. Liu, X. M. Guo, C. Tan, J. Li, Y. T. Kao, L. J. Wang, A. Sancar and D. P. Zhong, *J. Am. Chem. Soc.*, 2012, **134**, 8104.
25 Y. G. Ke, N. V. Voigt, K. V. Gothelf and W. M. Shih, *J. Am. Chem. Soc.*, 2012, **134**, 1770.
26 E. Laviron, *J. Electroanal. Chem.*, 1979, **100**, 263.
27 N. Tuleuova, C. N. Jones, J. Yan, E. Ramanculov, Y. Yokobayashi and A. Revzin, *Anal. Chem.*, 2010, **82**, 1851.
28 C. C. Chang, S. Lin, C. H. Lee, T. L. Chuang, P. R. Hsueh, H. C. Lai and C. W. Lin, *Biosens. Bioelectron.*, 2012, **37**, 68.
29 Y. Liu, J. Yan, M. C. Howland, T. Kwa and A. Revzin, *Anal. Chem.*, 2011, **83**, 8286.
30 J. J. Zhao, C. F. Chen, L. L. Zhang, J. H. Jiang and R. Q. Yu, *Biosens. Bioelectron.*, 2012, **36**, 129.
31 K. Min, M. Cho, S. Y. Han, Y. B. Shim, J. Ku and C. Ban, *Biosens. Bioelectron.*, 2008, **23**, 1819.